10-21-2017

Detection of Methylation on dsDNA Using Nanopores in MoS_2 Membrane

David Estrada
Boise State University

Detection of Methylation on dsDNA Using Nanopores in MoS_2 Membrane

Jiwook Shim [#,*]
Department of Biomedical Engineering
Rowan University
Glassboro, NJ
shimj@rowan.edu

Shouvik Banerjee [#]
Department of Material Science and Engineering
University of Illinois at Urbana – Champaign
Urbana, IL

Hu Qiu
State Key Laboratory of Mechanics and Control of Mechanical Structures
Nanjing University of Aeronautics and Astronautics
Nanjing, China

Kirby K. H. Smithe
Department of Electrical Engineering
Stanford University
Stanford, CA

David Estrada
Department of Material Science and Engineering
Boise State University
Boise, ID

Julian Bello
Department of Biomedical Engineering
Rowan University
Glassboro, NJ

Eric Pop
Department of Electrical Engineering
Stanford University
Stanford, CA

Klaus Schulten
Department of Physics and Beckman Institute
University of Illinois at Urbana – Champaign
Urbana, IL

and

Rashid Bashir*
Department of Bioengineering
University of Illinois at Urbana – Champaign
Urbana, IL

Micro and Nanotechnology Laboratory
University of Illinois at Urbana – Champaign
Urbana, IL

Carle Illinois College of Medicine
University of Illinois at Urbana – Champaign
Urbana, IL
rbashir@illinois.edu

[#]Authors equally contributed.

Abstract

Methylation at the 5-carbon position of the cytosine nucleotide base in DNA has been shown to be a precursor to carcinogenesis. Early detection of methylation and intervention could drastically increase the effectiveness of therapy and reduce the cancer mortality rate. Current methods for detecting methylation involve bisulfite genomic sequencing, which are cumbersome and demand a large sample size of bodily fluid to yield accurate results. Hence, more efficient and cost effective methods are desired. Building off our previous work, we present a novel nanopore-based assay using a nanopore in a MoS_2 membrane, and the methyl-binding protein (MBP), MBD1x, to detect methylation on dsDNA. We show that the dsDNA translocation was effectively slowed down using an asymmetric concentration of buffer and explore the possibility of profiling the position of methylcytosines on the DNA strands as they translocate through the 2D membrane. Our findings advance us one step closer towards the possible use of nanopore sensing technology in medical applications such as cancer detection.

Keywords: nanopore, molybdenum disulfide, methylated DNA, cancer detection, methyl-binding protein, hypermethylation, hypomethylation

Cancer research is often centered around early detection and finding tumors before they metastasize. DNA methylation, defined as the addition or removal of a methyl group at the 5-position of the cytosine nucleotide, has been established as an early event in carcinogenesis [1-3] with many promoter genes affected by aberrant methylation being linked to tumor formation. [4-6] In addition, high-throughput methylation analysis has unveiled that aberrant DNA methylation is correlated to both premalignant and malignant neoplasia. [7-10] Consequently, methylation pattern analysis in DNA can play a very critical role in the diagnosis of precancerous and early-stage cancer. However, current methods of analyzing genome-wide methylation rely heavily on bisulfite genomic sequencing. [11] This method requires a large sample volume due to DNA degradation during the bisulfite conversion and exhibits low PCR efficiency. [5, 12-13] Previous studies have reported the feasibility of detecting cancer by methylation pattern analysis from genomic extracts of human bodily fluids such as plasma, serum, urine, and stool. [5, 14-15] However, only a minuscule amount of methylated DNA can be obtained from body fluids. [13] As a result, most conventional methylation assays are not suitable for detecting the extremely low level of methylated DNA in bodily fluids. This presents a need for a less labor intensive and direct method to characterize methylation. Our previous work has successfully investigated the possibility of nanopore-based devices for detection of hypermethylation, coarse quantification of methylation sites, and coarse profiling of single dyad methylation pattern. Thus, we believe that the nanopore technology holds significant promise for detection of methylation for precancerous and early-stage cancer detection. [16-17]

Nanopore technology is a cost-effective, high-throughput platform that could assist in various medical applications such as immunoisolation bio capsules, drug delivery devices, and targeted biorecognition platforms. [18] Solid-state nanopores are favorable because they can operate in various liquid media and pH conditions as well as their production being scalable and compatible with other detection techniques [19-21] and other nanofabrication techniques. [22-23] However, certain obstacles, such as controlling translocation time and discriminating between bases and proteins, introduce complications that limit commercial use of the solid-state nanopore. In particular, they tend to exhibit relatively lower single molecule detection sensitivity due to the thickness of conventional membranes and inconsistent surface charge distribution.[22, 24-25] Although solid state nanopores yield low ionic current signal-to-noise ratios, graphene nanopores, in theory, can exhibit favorable detection sensitivity when compared to other solid-state nanopore such as SiN_x. [26] In this paper, we explore translocation of naked double-stranded DNA (dsDNA) and methylated dsDNA-MBP complex through nanopores drilled in a two-dimensional molybdenum disulfide (MoS_2) membrane. In addition, to attest to its viability as an alternative to graphene nanopores, we also present experiments with a buffer of asymmetric molarity to slow down translocation of biomolecules through the pore.

Results and Discussion

Fabrication and Current-Voltage Signature of the Nanopores in MoS_2

Solid-state nanopores can be used as inexpensive and high-performance biosensors that are capable of the single molecule detection of a wide variety of analytes of medical interest, ranging from small molecules to post-translationally modified proteins. [27] Specifically, the nanopore biosensing platform has become especially attractive in the realm of DNA sequencing. [22, 28] Nanopores use the principle of ionic current spectroscopy to electrically distinguish the unique current blockage signatures of each nucleotide base. [16, 29] Theoretically, the graphene nanogap of 1.6 nm would read the transverse conductance of the translocating DNA and could lead to an error-free read-out. [30] Atomically small graphene nanopores, closely resembling the diameter of dsDNA, have a high sensitivity to infinitesimal changes in the outer diameter of the translocating DNA. [31] These nanopores can resolve nanoscale-spaced molecular structures with a resolution of less than 0.6 nm along the length of the molecule. However, the unique density of the states of graphene and the absorption of water molecules are factors that could increase error in graphene nanopore readings. [30] more importantly, graphene nanopores have a strong hydrophobic interaction with ssDNA, which causes the DNA to attach to the graphene membrane and impedes translocation. [32] To overcome this, the surface of the graphene membrane often must be treated with agents such as 16-mercaptohexadecanoic acid in 8:2 toluene/ethanol to demote DNA adhesion and promote translocation. [24, 33-34]

Alternative materials have been explored to eliminate the need for additional surface treatment protocols. [22] Molybdenum disulfide is a novel atomically thin material that has been recognized as a possible alternative to graphene. As shown in Gaur et. al., MoS_2 membranes grown below 900 °C exhibit high surface energy and semi-crystalline structure that is associated with a decreased hydrophobicity and increased wetting. [35] The less hydrophobic surface nature of the MoS_2 grown under optimal conditions allows for successful threading of dsDNA of different

lengths and conformations, displaying superior yield. [24] MoS_2 nanopores also exhibit a lower failure rate at high ionic strength solutions,[24] and show four distinct ionic current signals for four homo-nucleobases.[22] Unlike graphene, the semiconducting bandgap of MoS_2 is independent of the width of the nano-ribbon and can allow for detection of changes in potential induced in the liquid environment due to the translocation of the DNA.

Figure 1a illustrates the layout of the MoS_2 nanopore structure that we have fabricated. The free standing MoS_2 monolayer was situated on a 12mm x 12mm substrate structure consisting of 300 nm thick SiN_x and 20 nm thick Al_2O_3 that were deposited using PECVD (plasma enhanced chemical vapor deposition) and ALD (atomic layer deposition). An 80-micron hole was opened on the backside of the silicon substrate using DRIE (deep reactive ion etching), and a concentric ~500 nm hole was subsequently opened through the Al_2O_3 using a FIB (focused ion beam) (See the Supporting Information for the detailed process). The MoS_2 membrane was grown using CVD (chemical vapor deposition) and transferred to the device, as described in Supporting Information, and the MoS_2 nanopore was subsequently drilled using TEM (transmission electron microscopy) as described in Methods Section. Figure 1b shows TEM image of a typical ~ 6 nm MoS_2 nanopore. Nanopores for this experiment were created between 4 nm and 6.5 nm in diameter, and the current-voltage characteristic of the MoS_2 nanopores were measured in both 1 M KCl and 0.6 M KCl as shown in figure 1c. Figure 1d shows a TEM image of free standing MoS_2 membrane over the FIB hole that confirms no defects were present on the membrane before drilling of the nanopore on the MoS_2 membrane. Also, high-resolution transmission electron microscopy (HRTEM) showed a honeycomb-like image that is unique to MoS_2, thus confirming that the MoS_2 membrane was properly grown by the CVD method, as shown in figure 1e. Additional characterizations were performed to analyze the quality of MoS_2 membrane using Raman Spectroscopy, as described in Supporting Information. The thickness of the MoS_2 membrane was examined by atomic force microscopy (AFM) as shown in Supporting Information. The height profile indicates that the thickness of the CVD grown MoS_2 membrane corresponds to the thickness of a single MoS_2 layer.

Detection of 10 kb Double-Stranded DNA

To examine the feasibility of translocating dsDNA through a MoS_2 nanopore, random sequences of 10 kbps dsDNA were introduced in a 6.5 nm MoS_2 nanopore. The dsDNA sequences were transported through the MoS_2 nanopore at various voltages in the buffer solution of 0.6M KCl at pH of 7.4 containing 10 mM Tris and 1 mM EDTA. Representative data traces of 10 kbps dsDNA transports at 500 mV, 700 mV, and 1000 mV are shown in figure 2a, 2b, and 2c. Distinct downward current blockages were observed in each of the data traces, undeniably confirming that the dsDNA transported through the MoS_2 nanopore. Figure 2d shows a scatter plot of all 10 kbps transports events at the displayed voltages. The data trace of 700 mV displayed higher dsDNA transport occurrence than that of the data trace of 500 mV, and the 1000 mV data trace showed more than that of the 700 mV data trace as expected. The higher occurrence of the dsDNA transport with increasing voltage is in agreeance with previous observations of dsDNA transports in SiN_x.[16] To further investigate the dsDNA transport through the MoS_2 nanopore, the current blockages and the translocation duration were analyzed. To obtain current blockage values of dsDNA transports, a histogram built with blocked current data produced by dsDNA transports was fitted with a Gaussian function as shown in figure 2e. The current blockages of 10 kb dsDNA through a 6.5 nm MoS_2 nanopore were 1.27 ± 0.24 nA at 500 mV, 1.7 ± 0.41 nA at 700 mV, and 2.35 ± 0.43 nA at 1000 mV. The amplitudes of current blockages were increased at higher biased voltages as shown in figure 2g, in agreement with the trends of dsDNA transport observed in other nanopores. [36-37] Figure 2f shows the transport duration values of the dsDNA which were obtained by fitting an exponential decay function to the dsDNA transport dwell time histograms. As expected, accelerated transport velocity was observed at higher biased voltages. The transport durations were 188 ± 17 µs at 500 mV, 118 ± 8 µs at 700 mV, and 83 ± 6 µs at 1000 mV as shown in figure 2h. As observed in dsDNA transport in other material nanopores, [16, 36-37] higher voltage generally yielded a stronger blockage current, but shorter transport duration times. Findings with 10 kbps dsDNA transports through the 6.5 nm MoS_2 nanopore were in concordance with observations in previous studies. Molecular dynamic (MD) simulations also demonstrated larger current blockages and reduced transport duration by transporting dsDNA through a MoS_2 nanopore at the higher voltages as shown in Supporting Information, thus validating our experimental findings. Previous studies have indicated the challenges of dsDNA transport through graphene nanopores due to the affinity of graphene surface to the DNA causing the DNA strand to adhere to the surface of the nanopore membrane. [36] Such difficulty was not observed on dsDNA transports through the MoS_2 nanopore in our studies as it was much less difficult to wet the nanopore membrane. However, a higher biased voltage, greater than 800 mV, can enlarge the open pore in the MoS2 nanopore[38] as was evident in a previous study after recording DNA transports at 1000 mV. Also, the enlarging of the MoS_2 nanopore can be seen in figure 2b and 2c, where occasional upward spikes

and increased noise level at 700 mV and 1000 mV were demonstrated. We have tested the current-voltage characteristic before and after applying 1000 mV, and the result indicate that the MoS_2 nanopore can be enlarged through electrochemical reaction (supporting information).

Detection of Naked and Methylated dsDNA Fragments

DNA methylation patterns are often correlated to tumor formation and cancer progression. Especially, previous studies reported that hypermethylation is associated with many types of cancer and potentially correlated with metastasis in many other tumor types. [5-6, 39-41] Previous studies have also demonstrated that nanopore sensors cannot discriminate between methylated DNA and unmethylated DNA without labeling of some sorts. [16] One method to utilize nanopore technology to detect methylation is to attach methyl binding proteins (MBPs) to the methylated DNA. MBPs selectively bind to the methylcytosine bases on methylated DNA, thereby confirming its presence in the sequence. [16-17] Our previous studies have presented the selective labeling of methylated sites on dsDNA using MBPs. Herein, we used the same strategy and DNA with the same methylated pattern to show the ability of the MoS_2 nanopore to discriminate naked DNA from hypermethylated DNA (hyMethDNA). Target DNA were 90 bp sequences with 30 *CpG* sites. No methylation was added to the naked DNA and 10 methylcytosine domains were added on hypermethylated DNA to have uniformly distributed methylation sites. For our experiment, a nanopore with a 7.2 nm diameter was used for detection of the 90bp dsDNA fragments in our nanopore experimental setup of 1M KCl at pH 7.2 containing 10 mM Tris and 1 mM EDTA. We first examined the detection of 90bp naked dsDNA through a MoS_2 nanopore at 200mV to prevent the MoS_2 nanopore from damage resulting from the enlargement of the nanopore at the high biased voltage. However, translocation events under these conditions were unnoticeable. Interestingly, upon lowering the applied voltage to 100 mV, transport events for the 90bp dsDNA were observed. It was surprising to see the transport of dsDNA through MoS_2 at these low biased voltages as other membranes typically require higher voltages to reveal translocation events. Representative transport sample events of 90bp dsDNA fragments through a MoS_2 nanopore are displayed in figure 3a, 3b, and 3c for applied voltages of 50mV, 80mV, and 100mV, respectively. To date, SiN_x and graphene nanopore experiments have not reported dsDNA transport below 200mV. Possible explanations for the lack of transportation data with these commonly used membranes could be the negative surface charge of the SiN_x membrane and the hydrophobic surface affinity to graphene causing DNA to adhere. This is especially relevant for the nanopores in SiN_x membranes ranging from 10~30 nm in thickness, where a smaller pore diameter than membrane thickness results in a pore that behaves like a nanochannel, increasing the entropic barrier that the DNA molecule needs to overcome to result in translocation. Since the isoelectric point of SiN_x is ~4 and negatively charged in experimental solution at pH 7.2, [42] the dsDNA would possibly be repelled at bias voltages under 200mV. In comparison, a pore in a thin MoS_2 2D membrane does not repel dsDNA. The values of transport current blockage and transport duration were obtained by fitting a Gaussian function, and an exponential decay function to the blocked current histogram and transport dwell time histogram respectively as demonstrated in figure 3d and 3e. The MoS_2 nanopore of 7.2 nm in diameter could detect 90bp dsDNA, with blocked current of 282 ± 22 pA at 50 mV, 312 ± 13 pA at 80 mV, and 376 ± 16 pA at 100 mV as shown in figure 3f and as well as dwell time of 53 ± 3 μs at 50mV, 36 ± 4 μs at 80 mV, and 32 ± 2 μs at 100mV as shown in figure 3g. The increase in the bias voltage to the original 200 mV did not result in noticeable transport events as demonstrated in figure 3h. However, the addition of hyMethDNA bound with MBD1x produced detectible events as shown in figure 3i. Representative sample events of hyMethDNA/MBD1x complex through the MoS_2 nanopore are presented in figure 3j. To form the complex of hyMethDNA and MBD1x, the two molecules were mixed and incubated at room temperature for 15 minutes before experiments. While recording when naked DNA was in the solution and no translocations were observed, hyMethDNA fully bound with MBD1x were introduced to the chamber. Surprisingly, the hyMethDNA with MBPs displayed a signature current blockage as shown in figure 3j and were selectively detected at 200mV. It can be inferred that the complex translocated through the pore slower than naked DNA due to the altered larger physical dimension brought on by annexing 10 MBD1x on the dsDNA fragment, in addition to the positive net charge of the MBD1x on the DNA reducing the overall charge on the complex. The isoelectric point of MBD1x is known to be 8.85, [43] thus it would be positively charged in the solution with pH 7.2. Not only does this serve as a confirmation of the presence of a methylcytosine base on the DNA sequence and the affinity of the MBP to the methyl group, but it also alludes to the ability of MoS_2 nanopores in detecting methylated DNA. The structure of the complex is presented in figure 3h to illustrate methylation and the presence of MBD1x in the DNA. The unmeasurable naked dsDNA transport events at 200mV (figure 3i) can be explained by translocation that was too rapid. The DNA translocation duration time was demonstrated to decrease at higher voltages in a voltage-dependent manner. Fitting with an exponential decay function (Supporting Information) shows the expected value of translocation of 90 bp dsDNA transport at 200 mV to be ~10 μs, which is close to the data acquisition time interval of 10 μs of the experimental setup (see methods section), and

hence was likely out of the measurement range. Figure 3l shows obtained current blockage and transport durations of naked DNA and hyMethDNA/MBD1x complex along with the expected current blockage and duration of 90bp dsDNA fragments transport at 200 mV, which is unnoticeable under our experimental recording condition.

Slowing Down dsDNA Transport and Detection of a Single CpG Site in dsDNA Fragment

Hypomethylation, the loss of methylation in DNA when compared to normal levels, is another major epigenetic modification in cancer cells. The pattern of DNA epigenetic alterations in cancer varies from the individual *CpG* dyad at the local level, to methylation in 1 million base pairs, to DNA demethylation during carcinogenesis. This results in loss of methylation on both strands via possible intermediates of hemimethylated dyads. [44]

However, conventional methylation assays such as methylation-specific PCR is technically limited and challenging for the diagnosis of DNA hypomethylation. [45] Although our previous study demonstrated discrimination between hypomethylated DNA and individual *CpG* dyad at the center of sequences by labeling with MBP, profiling of the methylation pattern using thick SiN_x membrane was not possible.[17] In that study, the single MBP was in the middle of the molecule and the electrical peak indicating the methylation location was broad. Herein, we report the methylation profile of dsDNA through a MoS_2 nanopore with a slow translocation velocity due to an asymmetric salt gradient.[46] Longer translocations can allow for high-resolution measurements to distinguish individual nucleotide bases.[47] Various strategies, from applying gel media on the cis or trans side of the membrane, to varying voltage or buffer solution concentration gradient, have been implemented to slow translocation and suspend DNA strands in the pore. [47-48] For our experiment, we used an asymmetric buffer solution of 0.6M KCl on the cis side of the membrane and 3M KCl on the trans side. Our MoS_2 nanopore-based methylation assay demonstrates detection of a single methylation *CpG* dyad site at the end of 90bp dsDNA. We utilized the MBD1x and chose a single methylation *CpG* dyad to check the viability of MoS_2 nanopore on detection of hypomethylated DNA. The target DNA fragments were designed to have a single *CpG* dyad methylated site near to the end of the strand, 84^{th} to 87^{th} bases in 90 bps dsDNA (endMethDNA). Both naked DNA and the endMethDNA bound with a single MBD1x were used for translocation experiments in a 9 nm MoS_2 nanopore and both displayed measurable current blockade signatures as shown in Figure 4a. Samples of 90bp naked DNA (Figure 4a top) and MBD1x bound endMethDNA (Figure 4a bottom) are shown in Figure 4a and the corresponding scatter plot is shown in Figure 4b. The transport current blockage values of both naked DNA, -277 ± 20 pA, and complex, -600 ± 66 pA, were obtained using a Gaussian function as shown in Figure 4c. The translocation times of naked DNA and the endMethDNA/MBD1x were also obtained by fitting a Gaussian function to transport dwell time histogram as shown in Figure 4d. In comparison to dsDNA transport in symmetric 1M KCl shown in Figure 3, using asymmetric salt gradient significantly slowed down the transport duration of 90bp naked DNA. Although direct comparison is not appropriate due to the large diameter of the nanopore used for this experiment, naked DNA was successfully detected with a duration of 1.23 ± 0.21 ms at 200 mV. In comparison with the expected transport in Figure 3l, the transport was slowed down ~100-fold. The endMethDNA bound with a single MBD1x translocated through the MoS_2 nanopore at 1.39 ± 0.23 ms, which was a ~160 µs slower translocation than the naked DNA. While we had previously found ~20-fold difference between naked DNA and locally methylated DNA through SiN_x nanopores, the similar range of translocation duration between naked DNA and endMethDNA was unexpected. However, the similar range of transport duration between naked DNA and endMethDNA/MBD1x can be explained. The negatively charged inner wall of a 10-nm thick SiN_x nanopore is likely to interact with the positively charged methyl-binding protein during transporting, whereas 2-D material MoS_2 nanopore is unlikely to interact during transporting. In addition, compared to hyMethDNA fully bound with MBD1x, endMethDNA possesses only one MBD1x. Thus the overall charge on the molecule is not perturbed. Consequently, the 90bp naked DNA and endMethDNA would not be significantly different in transport duration in the 2D MoS_2 membranes. The main factor impeding the complex transport through a MoS_2 nanopore is biased positive voltage. A demonstration of atomic-scale translocation dynamics of the complex through a MoS_2 nanopore is shown in Supporting Information. To further analyze the whole data set for the current blockade and transport duration, a box-and-whisker plot was adopted. Figure 4e shows that most current blockages of naked DNA fall in -276 ± 20 pA, and endMethDNA/MBD1x showed two distinct current blockage levels; shallow at -251 ± 39 pA and deeper at -600 ± 66 pA. The shallow current blockage is at similar levels of transport current blockage to that of naked DNA, thus corresponding to transport of DNA region on the complex. The deeper current blockages are associated with transport of MBD1x on the DNA through the nanopore. The ~3-fold increased current blockage by the MBP region is on the same order of magnitude as the current blockage found in previous studies as well.[16] The transport duration of naked DNA and endMethDNA bound with MBD1x is shown in Figure 4f. The transport of the MBP region on the DNA took 0.138 ± 0.11 ms. This translates to

10% of the entire complex translocation over a 139 ms period. Comprehensively, the MoS_2 nanopore can detect the methylation site more precisely than SiN_x membrane. The schematic in figure 4g illustrates dsDNA and endMethDNA bound with MBD1x. Slowed translocation times were observed by varying the buffer concentration.

Methylation site profiling shown in Figure 4h revealed that translocation events with the methylated DNA/MBD1x complex ended with the terminal protein instead of leading with it. It can be inferred from this finding that the positively charged MBD1x near the nanopore is always repelled by the positively applied bias voltage and will spin to the origin while the DNA region of the complex is being pulled into the nanopore. Consequently, all the endMethDNA/MBD1x transport into the pore occurred in a fixed orientation which included the DNA entering first and the protein complex lagging behind. From this, it can be assumed that the negatively charged DNA that was used for the study was attracted by the applied positive charge and pushed towards the nanopore ahead of the region where MBD1x was attached. This was confirmed through profiling of methylation location using the MoS_2 nanopore. The occurrence of deeper current blockage was mainly observed at the end of the whole complex transport, as shown in figure 4h. The abscissa represents the length of the entire complex translocation, normalized and recalculated as 100%. The peak occurrence of deeper current blockage was obtained by fitting a Gaussian function to the occurrence histogram. The fitting value was 90.5 ± 3% which indicates the deeper current blockages mainly occur at the end of entire complex translocation. This result suggests that the position of methylation on dsDNA can be more precisely detected using nanopores in thin membranes.

Conclusions

We investigate the use of the MoS_2 nanopore for dsDNA translocation and methylation detection experiments. Detection of methylcytosine bases has been reported previously with SiN_x and graphene nanopore sensors, but MoS_2 presents several favorable and specific characteristics that could make it a more viable and robust option than the more commonly used membranes. These characteristics include the ability to produce a small nanopore on a thin membrane while retaining good signal-to-noise ratios and no need for surface treatment to reduce hydrophobic surface interactions as is necessary for graphene membranes. After determining that dsDNA translocation was possible through MoS_2, we also showed that dsDNA translocation could be slowed by using asymmetric concentration of buffer solutions to provide higher spatial resolution. We demonstrated detection of single MBD1x proteins in a site-specific manner which could be used to distinguish the location of the methyl cytosine nucleotide base on the DNA sequence. We also hypothesized that the charge of the DNA strand coupled with the applied voltage allows one to control the orientation of the translocating DNA strand.

Being able to detect aberrant methylation in a routine lab screening could help identify cancer signatures at various stages or progression. This could prove crucial regarding early intervention and therapy and ultimately lead to an increase in the rate of survival. Work remains to be accomplished in the control of translocation speeds, resolution of signature current blockades, and in profiling the location of attached MBPs. We hope that this work serves as a springboard for future MoS_2 nanopore studies.

Materials and Methods

Supporting Substrate Fabrication

Substrates consisting of stacked layers of Al_2O_3 and SiN_x are fabricated on 300 ± 2 μm thick double-side polished <100> silicon wafers purchased from Silicon Quest International. Wafers are piranha cleaned (2:1 H_2SO_4/H_2O_2) for 20 min before deposition SiNx. 300 nm of low-stress SiN_x is deposited (STS Mesc PECVD system) using a mixed-frequency recipe (high frequency, 6 s at 13.56 MHz, platen power of 20 W; low frequency, 2s at 380 kHz, platen power of 60 W) with precursors SiH4 and NH3 at flow rates of 40 and 55 sccm, respectively, at a platen temperature of 300 °C. Subsequently, 20 nm of Al_2O_3 was deposited via ALD (Cambridge Nanotech) at a platen temperature of 250 °C using tetramethyl-aluminum (TMA) and water vapor precursor. Optical lithography is used to define square windows of 80 μm on the back side of the wafer with the aid of plasma resistant Megaposit SPR-220 photoresist and an ABM Flood Exposure (model 60) tool. Then the wafer is placed inside an STS Pegasus ICP (inductively coupled plasma) DRIE and 80 μm square membranes are suspended using a Bosch etching process; 500 to 600 nm holes are then drilled in these membranes using a focused ion beam (FIB) (FEI DB235) operated at a beam current of 30 pA.

Chemical Vapor Deposition of Molybdenum Disulfide

The detailed process of growing and characterizing of the MoS_2 film using Chemical Vapor Deposition on SiO_2 and Sapphire substrates are described in previous studies. [49-50]

Nanopore Fabrication, Chemicals, and Materials.

Single nanopores of various diameters were drilled in the free standing MoS_2 membrane on the supporting substrate with condensed electron beam using a JEOL 2010F field-emission gun TEM operated at 200kV in CBD mode with focused electron probe of diameter at 1.6 nm. All custom DNA fragments were synthesized, purified and purchased form Integrated DNA Technologies (Coralville, IA). The electrical nanopore measurements were performed in 0.6 M, 1 M, and 0.6 M / 3 M KCl at pH 7.2 containing 10 mM Tris and 1 mM ethylenediaminetetraacetic acid (EDTA) for naked DNA fragments and DNA fragments bound with MBD1x. The methylated DNA/MBD1x complexes were prepared and incubated for 15 min at room temperature (25 ± 2°C) immediately before the nanopore experiments.

MBD1x Protein Purification

MBD1x purification was described in a previous report. [16]

Nanopore Electrical Measurements

The nanopore chip was assembled in a custom-built chamber. Ethanol was then filled in reservoirs of both chambers initially to clean the device and promote wetting. Subsequently, the ethanol was flushed out with deionized water and the reservoirs are filled with desired experimental salt solutions. Ag/AgCl electrodes are immersed in reservoirs for ionic current measurements. All nanopore experiments are performed with Axopatch 200B and Digidata 1440A at room temperature (25 ± 2°C). Axopatch 200B was used for applying biased voltages and measuring currents through a nanopore, and data were recorded using a Digidata 1440A acquisition system. Data were low-pass filtered at 10 kHz using the built in 8-pole Bessel filter, and recorded at 100 kHz sampling rates. Clampex 10.2 was used for instrumental control, and Clampfit 10.2 was used for data analysis. All nanopore experiments are performed on an antivibration table in a dark double Faraday cage.

MD Simulations

The dsDNA was created by the X3DNA program [51]. The atomic structure of the terminal-methylated DNA molecule/MBD1 complex was constructed by linking dsDNA fragments to the ends of DNA molecule in the reported crystal structure of the mDNA-MBD1 complex (pdb code:1IG4) [52]

All molecular dynamics simulations were carried out using NAMD [53], with protein and DNA described by the CHARMM22 force field with CMAP corrections and the CHMARMM27 force field, respectively [54]. Water was modeled with the TIP3P water model [55]. An integration time step of 2 s was adopted. Long-range Coulomb interactions were computed using the particle-mesh Ewald (PME) method [56]. The system was energy minimized for 5000 steps, then heated to 300 K. A 2 ns equilibration under NPT ensemble conditions was performed to equilibrate the system to a desired pressure of 1 atm, during which the temperature was maintained by applying Langevin dynamics and the pressure was maintained by a Nose-Hoover Langevin piston method [57]. This equilibration step was followed by a 4 ns equilibration under NVT ensemble condition. After the equilibration, an external electric field was applied along the z direction to drive the transport of biomolecules through MoS_2 nanopores.

Acknowledgement

J.B. and J.S are supported by Rowan University Startup Fund. H.Q. acknowledges the support by National NSF of China (11402113) and Jiangsu NSF (BK20140807). R.B. acknowledges support from Oxford Nanopore Technologies U.K. and from Mayo-Illinois Alliance for Technology Based Healthcare (http://mayoillinois.org/) for supporting J.S., and S.B.

References

1. Fearon, E. R.; Vogelstein, B., A genetic model for colorectal tumorigenesis. *Cell 61* (5), 759-767.
2. Baylin, S. B.; Herman, J. G.; Graff, J. R.; Vertino, P. M.; Issa, J. P., Alterations in DNA methylation: a fundamental aspect of neoplasia. *Adv Cancer Res* **1998,** *72*, 141-96.
3. Li, E.; Bestor, T. H.; Jaenisch, R., Targeted mutation of the DNA methyltransferase gene results in embryonic lethality. *Cell 69* (6), 915-926.
4. Laird, P. W.; Jaenisch, R., The role of DNA methylation in cancer genetic and epigenetics. *Annu Rev Genet* **1996,** *30*, 441-64.
5. Laird, P. W., The power and the promise of DNA methylation markers. *Nat Rev Cancer* **2003,** *3* (4), 253-266.
6. Esteller, M.; Corn, P. G.; Baylin, S. B.; Herman, J. G., A Gene Hypermethylation Profile of Human Cancer. *Cancer Research* **2001,** *61* (8), 3225.
7. Adorjan, P.; Distler, J.; Lipscher, E.; Model, F.; Muller, J.; Pelet, C.; Braun, A.; Florl, A. R.; Gutig, D.; Grabs, G.; Howe, A.; Kursar, M.; Lesche, R.; Leu, E.; Lewin, A.; Maier, S.; Muller, V.; Otto, T.; Scholz, C.; Schulz, W. A.; Seifert, H. H.; Schwope, I.; Ziebarth, H.; Berlin, K.; Piepenbrock, C.; Olek, A., Tumour class prediction and discovery by microarray-based DNA methylation analysis. *Nucleic Acids Res* **2002,** *30* (5), e21.
8. Iacobuzio-Donahue, C. A.; Maitra, A.; Olsen, M.; Lowe, A. W.; van Heek, N. T.; Rosty, C.; Walter, K.; Sato, N.; Parker, A.; Ashfaq, R.; Jaffee, E.; Ryu, B.; Jones, J.; Eshleman, J. R.; Yeo, C. J.; Cameron, J. L.; Kern, S. E.; Hruban, R. H.; Brown, P. O.; Goggins, M., Exploration of global gene expression patterns in pancreatic adenocarcinoma using cDNA microarrays. *Am J Pathol* **2003,** *162* (4), 1151-62.
9. Goelz, S. E.; Vogelstein, B.; Hamilton, S. R.; Feinberg, A. P., Hypomethylation of DNA from benign and malignant human colon neoplasms. *Science* **1985,** *228* (4696), 187-90.
10. Feinberg, A. P.; Gehrke, C. W.; Kuo, K. C.; Ehrlich, M., Reduced genomic 5-methylcytosine content in human colonic neoplasia. *Cancer Res* **1988,** *48* (5), 1159-61.
11. Murrell, A.; Rakyan, V. K.; Beck, S., From genome to epigenome. *Human Molecular Genetics* **2005,** *14* (suppl 1), R3-R10.
12. Murrell, A.; Rakyan, V. K.; Beck, S., From genome to epigenome. *Hum Mol Genet* **2005,** *14 Spec No 1*, R3-R10.
13. Grunau, C.; Renault, E.; Rosenthal, A.; Roizes, G., MethDB--a public database for DNA methylation data. *Nucleic Acids Res* **2001,** *29* (1), 270-4.
14. Kisiel, J. B.; Yab, T. C.; Taylor, W. R.; Chari, S. T.; Petersen, G. M.; Mahoney, D. W.; Ahlquist, D. A., Stool DNA testing for the detection of pancreatic cancer Assessment of Methylation Marker Candidates. *Cancer* **2012,** *118* (10), 2623-2631.
15. Kandimalla, R.; van Tilborg, A. A.; Zwarthoff, E. C., DNA methylation-based biomarkers in bladder cancer. *Nature Reviews Urology* **2013,** *10* (6), 327-335.
16. Shim, J.; Humphreys, G. I.; Venkatesan, B. M.; Munz, J. M.; Zou, X.; Sathe, C.; Schulten, K.; Kosari, F.; Nardulli, A. M.; Vasmatzis, G.; Bashir, R., Detection and Quantification of Methylation in DNA using Solid-State Nanopores. *Scientific Reports* **2013,** *3*, 1389.
17. Shim, J.; Kim, Y.; Humphreys, G. I.; Nardulli, A. M.; Kosari, F.; Vasmatzis, G.; Taylor, W. R.; Ahlquist, D. A.; Myong, S.; Bashir, R., Nanopore-Based Assay for Detection of Methylation in Double-Stranded DNA Fragments. *ACS Nano* **2015,** *9* (1), 290-300.
18. Desai, T. A.; Hansford, D. J.; Kulinsky, L.; Nashat, A. H.; Rasi, G.; Tu, J.; Wang, Y.; Zhang, M.; Ferrari, M., Nanopore Technology for Biomedical Applications. *Biomedical Microdevices* **1999,** *2* (1), 11-40.
19. Kurz, V.; Nelson, E. M.; Shim, J.; Timp, G., Direct visualization of single-molecule translocations through synthetic nanopores comparable in size to a molecule. *ACS Nano* **2013,** *7* (5), 4057-69.
20. Nelson, E. M.; Kurz, V.; Shim, J.; Timp, W.; Timp, G., Using a nanopore for single molecule detection and single cell transfection. *Analyst* **2012,** *137* (13), 3020-7.
21. Soni, G. V.; Singer, A.; Yu, Z.; Sun, Y.; McNally, B.; Meller, A., Synchronous optical and electrical detection of biomolecules traversing through solid-state nanopores. *Rev Sci Instrum* **2010,** *81* (1), 014301.
22. Feng, J.; Liu, K.; Bulushev, R. D.; Khlybov, S.; Dumcenco, D.; Kis, A.; Radenovic, A., Identification of single nucleotides in MoS2 nanopores. *Nat Nano* **2015,** *10* (12), 1070-1076.
23. Banerjee, S.; Shim, J.; Rivera, J.; Jin, X.; Estrada, D.; Solovyeva, V.; You, X.; Pak, J.; Pop, E.; Aluru, N.; Bashir, R., Electrochemistry at the edge of a single graphene layer in a nanopore. *ACS Nano* **2013,** *7* (1), 834-43.

24. Liu, K.; Feng, J.; Kis, A.; Radenovic, A., Atomically Thin Molybdenum Disulfide Nanopores with High Sensitivity for DNA Translocation. *ACS Nano* **2014,** *8* (3), 2504-2511.
25. Merchant, C. A.; Healy, K.; Wanunu, M.; Ray, V.; Peterman, N.; Bartel, J.; Fischbein, M. D.; Venta, K.; Luo, Z.; Johnson, A. T. C.; Drndić, M., DNA Translocation through Graphene Nanopores. *Nano Letters* **2010,** *10* (8), 2915-2921.
26. Fyta, M., Threading DNA through nanopores for biosensing applications. *Journal of Physics-Condensed Matter* **2015,** *27* (27).
27. Bayley, H., Nanopore Sequencing: From Imagination to Reality. *Clinical Chemistry* **2014,** *61* (1), 25.
28. Venta, K.; Shemer, G.; Puster, M.; Rodriguez-Manzo, J. A.; Balan, A.; Rosenstein, J. K.; Shepard, K.; Drndic, M., Differentiation of short, single-stranded DNA homopolymers in solid-state nanopores. *ACS Nano* **2013,** *7* (5), 4629-36.
29. Li, J.; Yu, D.; Zhao, Q., Solid-state nanopore-based DNA single molecule detection and sequencing. *Microchimica Acta* **2016,** *183* (3), 941-953.
30. Postma, H. W. C., Rapid Sequencing of Individual DNA Molecules in Graphene Nanogaps. *Nano Letters* **2010,** *10* (2), 420-425.
31. Garaj, S.; Liu, S.; Golovchenko, J. A.; Branton, D., Molecule-hugging graphene nanopores. *Proceedings of the National Academy of Sciences* **2013,** *110* (30), 12192-12196.
32. Sathe, C.; Zou, X.; Leburton, J.-P.; Schulten, K., Computational Investigation of DNA Detection Using Graphene Nanopores. *ACS Nano* **2011,** *5* (11), 8842-8851.
33. Farimani, A. B.; Min, K.; Aluru, N. R., DNA Base Detection Using a Single-Layer MoS2. *ACS Nano* **2014,** *8* (8), 7914-7922.
34. Schneider, G. F.; Kowalczyk, S. W.; Calado, V. E.; Pandraud, G.; Zandbergen, H. W.; Vandersypen, L. M. K.; Dekker, C., DNA Translocation through Graphene Nanopores. *Nano Letters* **2010,** *10* (8), 3163-3167.
35. Gaur, A. P. S.; Sahoo, S.; Ahmadi, M.; Dash, S. P.; Guinel, M. J. F.; Katiyar, R. S., Surface Energy Engineering for Tunable Wettability through Controlled Synthesis of MoS2. *Nano Letters* **2014,** *14* (8), 4314-4321.
36. Banerjee, S.; Wilson, J.; Shim, J.; Shankla, M.; Corbin, E. A.; Aksimentiev, A.; Bashir, R., Slowing DNA Transport Using Graphene-DNA Interactions. *Advanced Functional Materials* **2015,** *25* (6), 936-946.
37. Shim, J.; Rivera, J. A.; Bashir, R., Electron beam induced local crystallization of HfO2 nanopores for biosensing applications. *Nanoscale* **2013,** *5* (22), 10887-10893.
38. Feng, J.; Liu, K.; Graf, M.; Lihter, M.; Bulushev, R. D.; Dumcenco, D.; Alexander, D. T.; Krasnozhon, D.; Vuletic, T.; Kis, A.; Radenovic, A., Electrochemical Reaction in Single Layer MoS2: Nanopores Opened Atom by Atom. *Nano Lett* **2015,** *15* (5), 3431-8.
39. Das, P. M.; Singal, R., DNA methylation and cancer. *J Clin Oncol* **2004,** *22* (22), 4632-42.
40. Strathdee, G.; Brown, R., Aberrant DNA methylation in cancer: potential clinical interventions. *Expert Rev Mol Med* **2002,** *4* (4), 1-17.
41. Vanaja, D. K.; Ehrich, M.; Van den Boom, D.; Cheville, J. C.; Karnes, R. J.; Tindall, D. J.; Cantor, C. R.; Young, C. Y., Hypermethylation of genes for diagnosis and risk stratification of prostate cancer. *Cancer Invest* **2009,** *27* (5), 549-60.
42. Hoogerheide, D. P.; Garaj, S.; Golovchenko, J. A., Probing surface charge fluctuations with solid-state nanopores. *Phys Rev Lett* **2009,** *102* (25), 256804.
43. Jorgensen, H. F.; Adie, K.; Chaubert, P.; Bird, A. P., Engineering a high-affinity methyl-CpG-binding protein. *Nucleic Acids Res* **2006,** *34* (13), e96.
44. Ehrlich, M., DNA hypomethylation in cancer cells. *Epigenomics* **2009,** *1* (2), 239-59.
45. Krausz, C.; Sandoval, J.; Sayols, S.; Chianese, C.; Giachini, C.; Heyn, H.; Esteller, M., Novel insights into DNA methylation features in spermatozoa: stability and peculiarities. *PLoS One* **2012,** *7* (10), e44479.
46. Wanunu, M.; Morrison, W.; Rabin, Y.; Grosberg, A. Y.; Meller, A., Electrostatic focusing of unlabelled DNA into nanoscale pores using a salt gradient. *Nat Nanotechnol* **2010,** *5* (2), 160-5.
47. Waugh, M.; Carlsen, A.; Sean, D.; Slater, G. W.; Briggs, K.; Kwok, H.; Tabard-Cossa, V., Interfacing solid-state nanopores with gel media to slow DNA translocations. *ELECTROPHORESIS* **2015,** *36* (15), 1759-1767.
48. Kyle, B.; Martin, C.; Harold, K.; Timothea, L.; Sanmeet, C.; José, B.; Matthew, W.; Vincent, T.-C., Kinetics of nanopore fabrication during controlled breakdown of dielectric membranes in solution. *Nanotechnology* **2015,** *26* (8), 084004.

49. Dumcenco, D.; Ovchinnikov, D.; Marinov, K.; Lazic, P.; Gibertini, M.; Marzari, N.; Lopez Sanchez, O.; Kung, Y. C.; Krasnozhon, D.; Chen, M. W.; Bertolazzi, S.; Gillet, P.; Fontcuberta i Morral, A.; Radenovic, A.; Kis, A., Large-Area Epitaxial Monolayer MoS2. *ACS Nano* **2015,** *9* (4), 4611-20.
50. Kirby, K. H. S.; Chris, D. E.; Saurabh, V. S.; Eric, P., Intrinsic electrical transport and performance projections of synthetic monolayer MoS 2 devices. *2D Materials* **2017,** *4* (1), 011009.
51. Lu, X. J.; Olson, W. K., 3DNA: a software package for the analysis, rebuilding and visualization of three-dimensional nucleic acid structures. *Nucleic Acids Research* **2003,** *31* (17), 5108-5121.
52. Ohki, I.; Shimotake, N.; Fujita, N.; Jee, J.-G.; Ikegami, T.; Nakao, M.; Shirakawa, M., Solution Structure of the Methyl-CpG Binding Domain of Human MBD1 in Complex with Methylated DNA. *Cell* **2001,** *105* (4), 487-497.
53. Kale, L.; Skeel, R.; Bhandarkar, M.; Brunner, R.; Gursoy, A.; Krawetz, N.; Phillips, J.; Shinozaki, A.; Varadarajan, K.; Schulten, K., NAMD2: Greater scalability for parallel molecular dynamics. *Journal of Computational Physics* **1999,** *151* (1), 283-312.
54. MacKerell, A. D.; Bashford, D.; Bellott, M.; Dunbrack, R. L.; Evanseck, J. D.; Field, M. J.; Fischer, S.; Gao, J.; Guo, H.; Ha, S.; Joseph-McCarthy, D.; Kuchnir, L.; Kuczera, K.; Lau, F. T. K.; Mattos, C.; Michnick, S.; Ngo, T.; Nguyen, D. T.; Prodhom, B.; Reiher, W. E.; Roux, B.; Schlenkrich, M.; Smith, J. C.; Stote, R.; Straub, J.; Watanabe, M.; Wiorkiewicz-Kuczera, J.; Yin, D.; Karplus, M., All-atom empirical potential for molecular modeling and dynamics studies of proteins. *Journal of Physical Chemistry B* **1998,** *102* (18), 3586-3616.
55. Jorgensen, W. L.; Chandrasekhar, J.; Madura, J. D.; Impey, R. W.; Klein, M. L., Comparison of simple potential functions for simulating liquid water. *The Journal of Chemical Physics* **1983,** *79* (2), 926-935.
56. Essmann, U.; Perera, L.; Berkowitz, M. L.; Darden, T.; Lee, H.; Pedersen, L. G., A smooth particle mesh Ewald method. *The Journal of Chemical Physics* **1995,** *103* (19), 8577-8593.
57. Feller, S. E.; Zhang, Y.; Pastor, R. W.; Brooks, B. R., Constant pressure molecular dynamics simulation: The Langevin piston method. *The Journal of Chemical Physics* **1995,** *103* (11), 4613-4621.

Figure 1

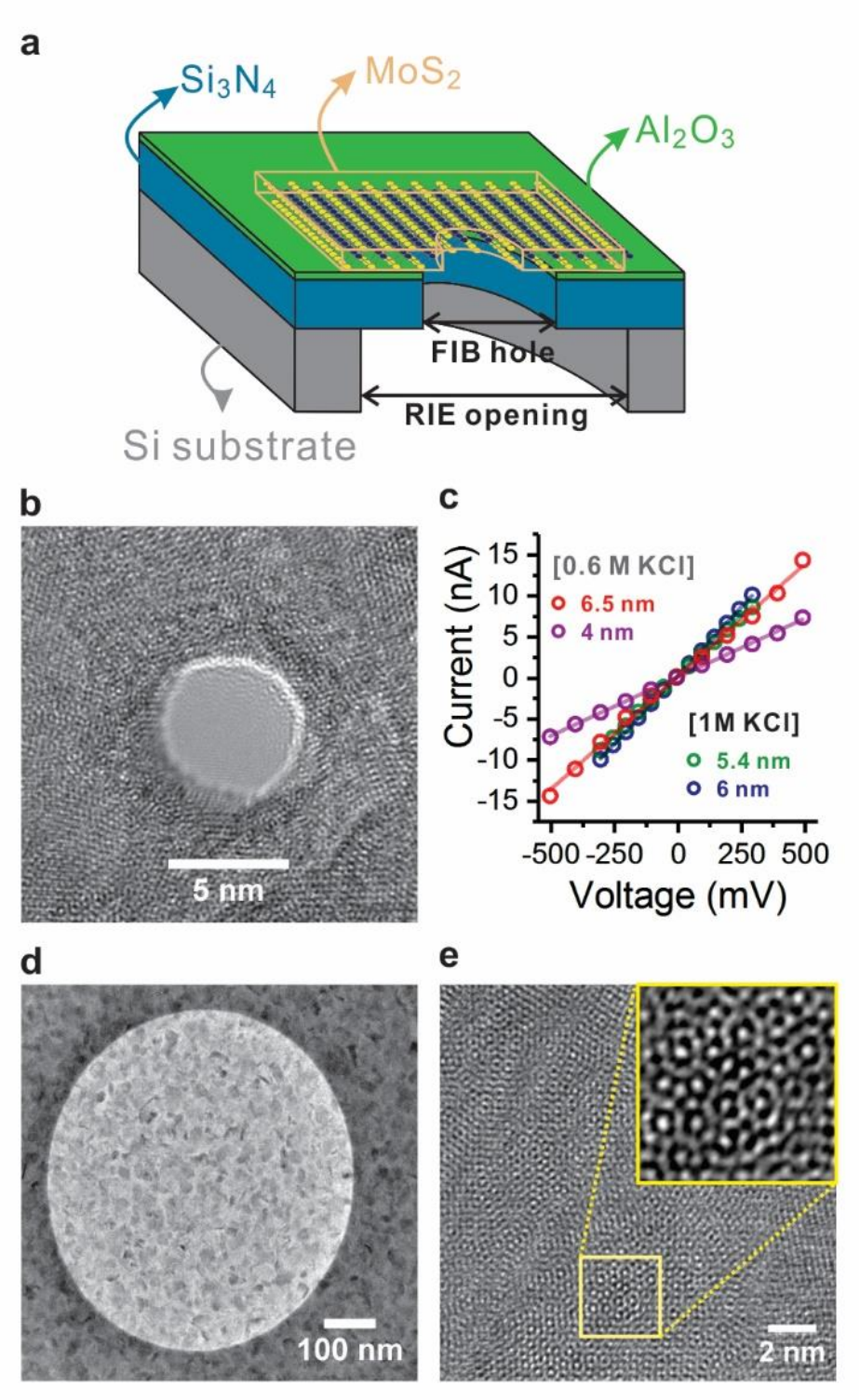

Figure 2.

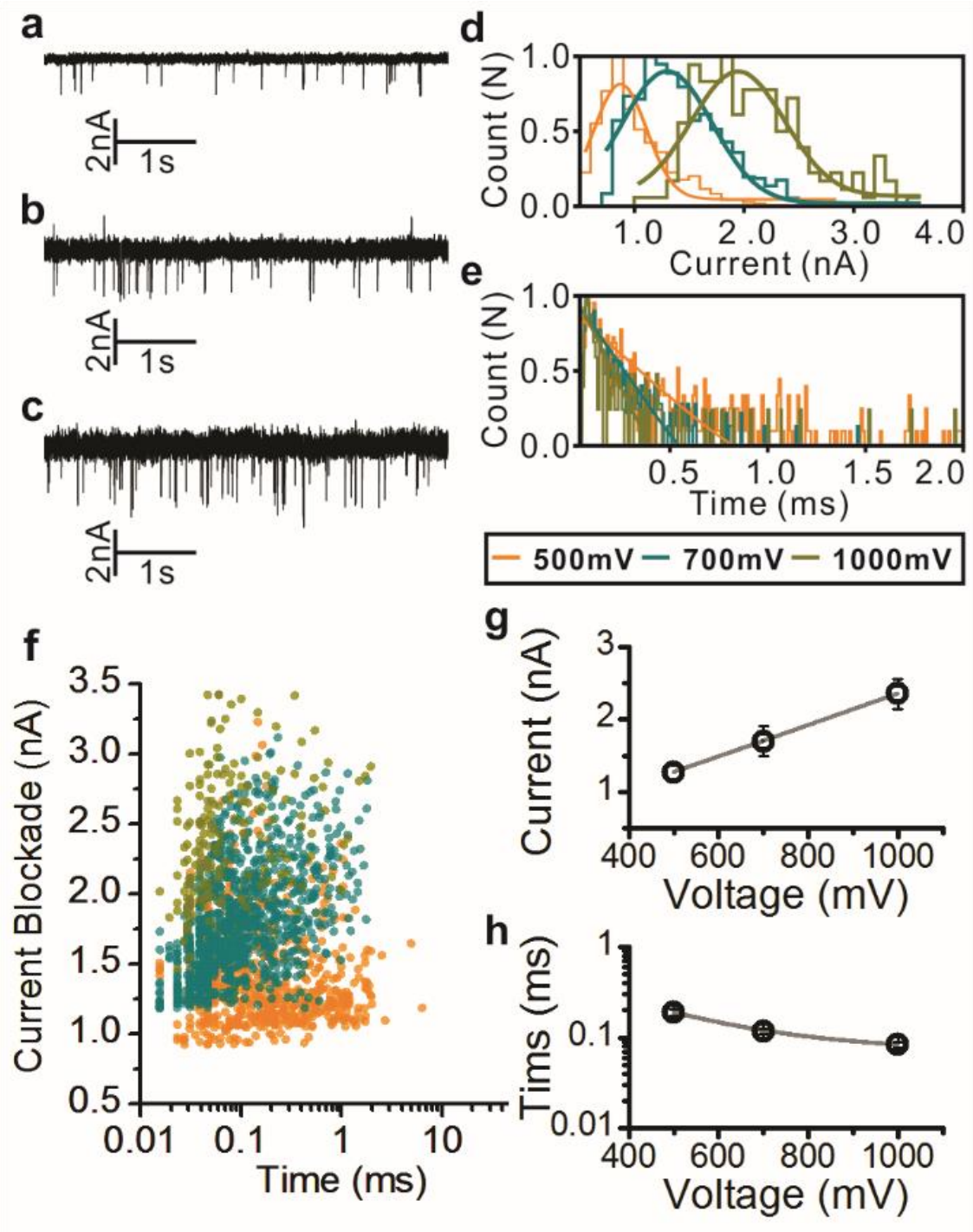

Figure 3.

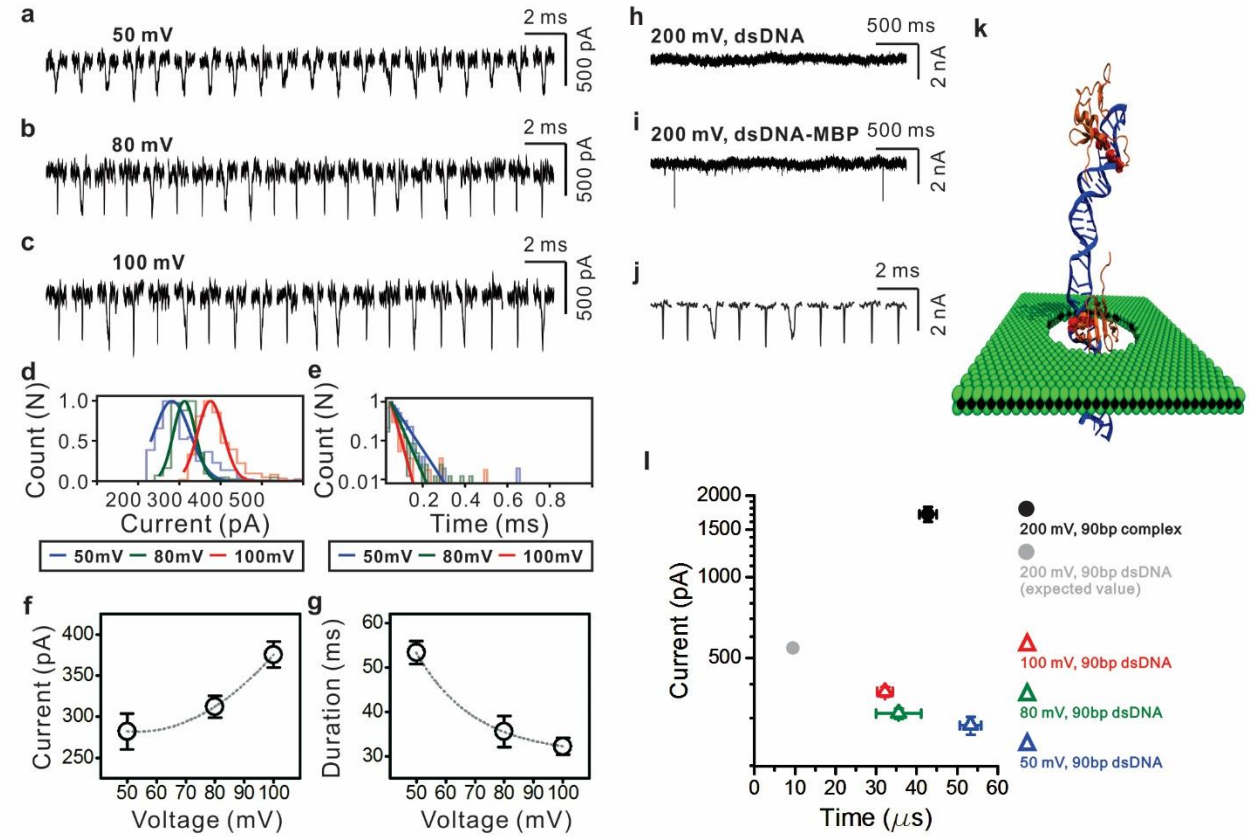

Figure 4.

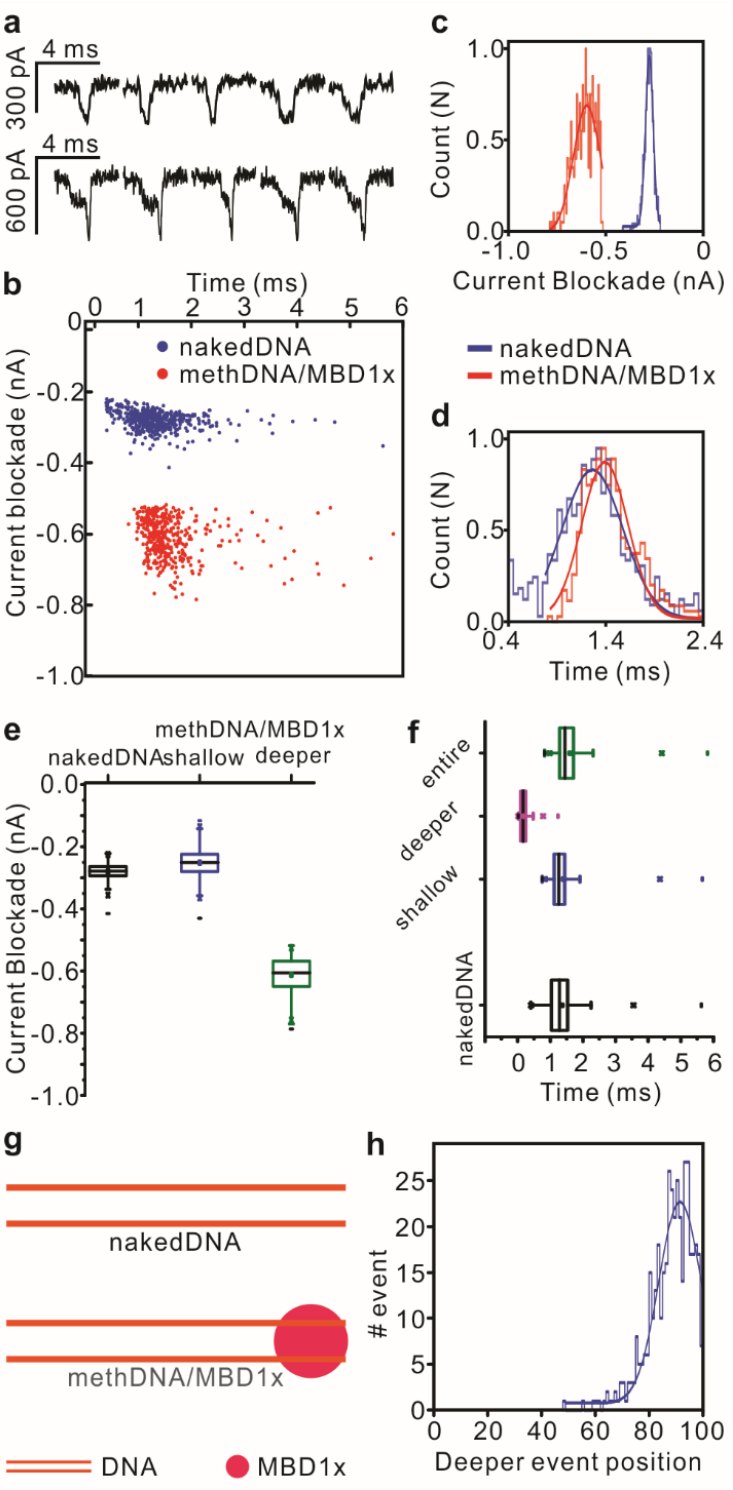

Figure Captions

Figure 1. a. Schematic illustrates the MoS2 nanopore structure. b. TEM image of typical 6 nm MoS2 nanopore. c. IV characteristic of MoS2 nanopores in KCl solution at pH 7.2 containing 10 mM Tris and 1 mM EDTA. d. TEM image shows that MoS2 layer covers entire FIB pore of 600nm diameter. e. HRTEM shows honeycomb-like MoS2 membrane structure. (inlet shows zoomed-in image of yellow square).

Figure 2. a. Data trace of 10 kbps dsDNA transport at 500 mV. b. Data trace of 10 kbps dsDNA transport at 700 mV. c. Data trace of 10 kbps dsDNA transport at 1000 mV. d. Scatter plotting of 10 kbps dsDNA transports in 6.5 nm MoS2 nanopore at 600mM KCl solution at pH 7.4 containing 10 mM Tris and 1 mM EDTA. e. Current blockade histogram. f. Transport duration histogram. g. Current blockades of DNA transports h. Transport durations of DNA transports.

Figure 3. a. Sample events of 90 bps dsDNA transports at 50 mV biased voltage in 9 nm MoS2 nanopore. b. Sample events of 90 bps dsDNA transports at 80 mV biased voltage in 9 nm MoS2 nanopore. c. Sample events of 90bps dsDNA transports at 100 mV biased voltage in 9 nm MoS2 nanopore. d. Current blockage histogram in the function of biased voltages. e. Blocked current duration histogram in the function of biased voltages. f. Current blockade of transports. The values are obtained by fitting Gaussian function to the current blokdade histogram. g. Blocked current duration of transports. The values are obtained by fitting the exponential decay function to the blocked current duration histogram. h. Current trace of 90 bp dsDNA transport at 200 mV biased voltage in 9 nm MoS2 nanopore. Momentary transport duration of short DNA is beyond of detection limit of measurement device, consequently transports of 90 bp dsDNA were undetectible. i. Current trace of 90 bp methylated dsDNA-MBP transports at 200 mV biased voltage in 9 nm MoS2 nanopore. j. Sample events of 90 bp methylated dsDNA-MBP transports at 200 mV in 9 nm MoS2 nanopore. k. Still image of molecular dynamic simulation showing methylated dsDNA-MBP complex transport through MoS2 nanopore. l. Transports data comparison between dsDNA and methylated DNA-MBP.

Figure 4. a. Sample transport events of naked DNA (top) and terminal-methDNA/MBD1x (bottom) in asymmetric solution. b. scatter plotting of transport events. Blue dots represent naked DNA transport and red dots represent the complex. c. Current blockade histogram of naked DNA (blue) and complex (red) transport. d. Transport duration histogram of naked DNA (blue) and complex (red) events. e. Box chart of current blockades. Current blockade of naked DNA is shown in block, DNA region of complex (shallow) is in blue, and DNA/ protein region (deeper) in green. f. Box chart of transport durations. Transport duration of naked DNA is shown in black, DNA region of complex (shallow) in blue, DNA/protein region (deeper) in red, and entire complex in green. g. Schematic shows scaled dsDNA and methDNA/MBD1x complex. h. Methylation site profiling shows that most complex transports end with terminal-protein. It is hypothesized that negatively charged DNA enters the nanopore by applied positive voltage and transport ends with protein.

Supporting Information

Supplementary Information Figure S1

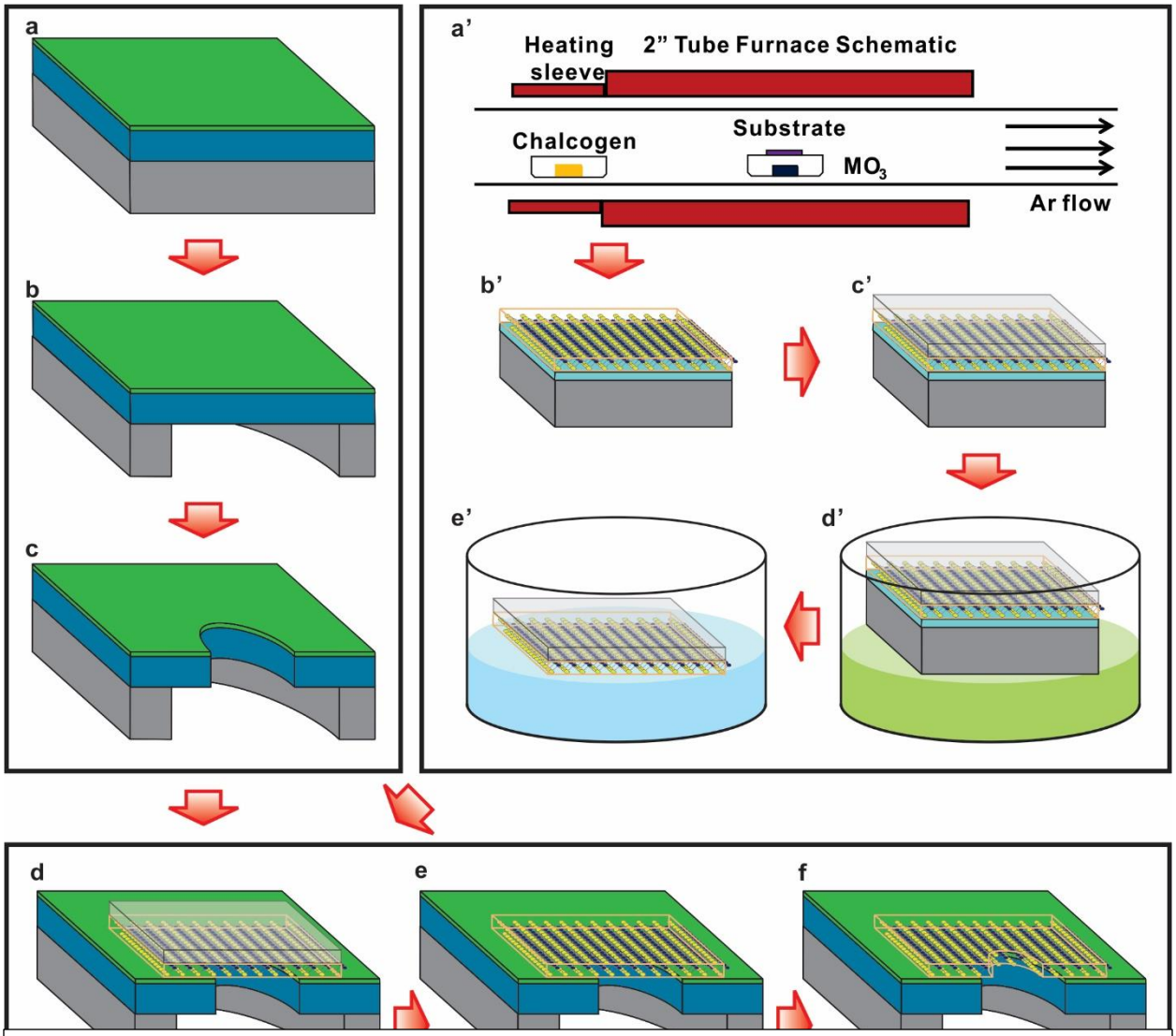

This is an author-produced, peer-reviewed version of this article. The final, definitive version of this document can be found online at *Nanoscale*, published by Royal Society of Chemistry. Copyright restrictions may apply. doi: 10.1039/C7NR03092D

Figure S1. Detailed process of fabricating free-standing MoS_2 membrane nanopore on the supporting substrate. a. Membranes consisting of stacked layers of SiN_x and Al2O3 are fabricated on 300 ± 2 µm thick double-side polished <100> silicon wafers purchased from Silicon Quest international. Before deposition of stacked layers, wafers are piranha cleaned (2:1 H2SO4/H2O2) for 20 min on a 120 °C hotplate. 300 nm of low-stress SiNx is deposited using STS Mesc PECVD system on the silicon substrate at a mixed-frequency recipe (high frequency, 6 s at 13.56 Mhz, platen power of 20 W; and low frequency, 2 s at 380 kHz, platen power of 60W) with precursors SiH4 and NH3 at flow rates of 40 and 55 sccm, respectively, at a platen temperature of 300 °C. Subsequently 20 nm-thick Al_2O_3 was deposited at a paten temperature of 250 °C via ALD (Cambridge Nanotech) using tetramethyl-aluminum (TMA) and water vapor precursors. b. Optical lithography is used to define 80 µm square windows on the back side of the wafer with the aid of plasma resistant megaposit SPR-220 photoresist and an ABM Flood Exposure (Model 60) tool. The wafer is then placed inside an STS Pegasus ICP DRIC and 80 µm square membranes are suspended using a Bosch etching process. c. 500 to 600 nm holes are sculpted in these membranes using a focused ion beam (FIB, FEI DB235) operated at a beam current of 30 pA. a'. For MoS_2 growth, the substrate is placed face-down over a crucible containing

~1 mg of MoO_3 powder, and solid sulfur pieces are placed ~26 cm upstream. After evacuating the tube to <1 Torr, the tube is filled to 760 Torr with Ar. The Ar flow is then reduced to 30 sccm for the growth. Synthesis on SiO_2 is done as in Ref. S1, whereas synthesis on sapphire was done in a similar manner as Ref. S2. b'. The MoS_2 film is then removed from the furnace. c'. PMMA (A4 950K) is coated on the MoS_2 film by using spin coater at 3000 rpm followed by baking at 200 °C for 10 min. After 15 min cooling down, second PMMA layer was coated using the same parameters. d'. PMMA coated MoS_2 film on SiO_2 or Sapphire substrate was then floated on the 1M KOH at 80 °C for 1 hour till MoS_2/PMMA stack delaminates. e' PMMA coated MoS_2 film is detached from the substrate. d. The detached PMMA/ MoS_2 layers are transferred to supporting substrate after rinsing with DIH2O, and dried at room temperature for 2 hours. Subsequently, the substrate is placed on a hot plate at room temperature and ramp to 150 °C for 20 min. e. The PMMA layer was dissolved in acetone for 30 min, rinsed with IPA, washed with DIH2O. Then, the samples are heated in Ar/H2 atmosphere for 1.5 hours at 400 °C. f. A nanopore was drilled on the MoS_2 membrane as described in Methods.

Supplementary Information Figure S2

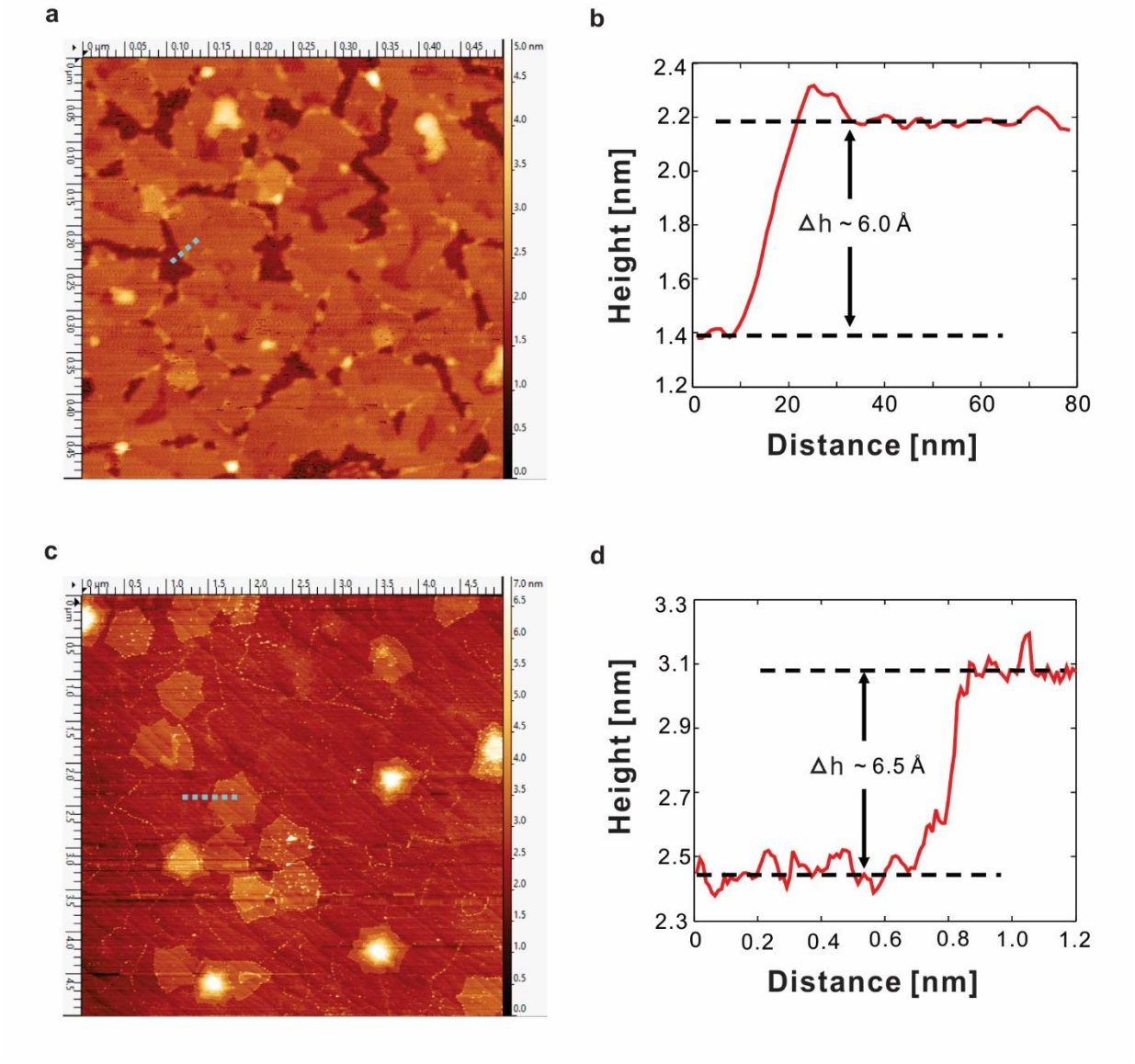

Figure S2. (a) and (b): AFM image and height profile of a subcontinuous MoS_2 growth on sapphire showing the monolayer height of ~6 Å. (c) and (d): AFM image and height profile of a continuous growth on sapphire, showing small overgrowth regions with a 1L-2L height of ~6.5 Å. Also note the ridges in Fig. S2c, which are the terraces of the reconstructed sapphire surface, as in Ref. S2.

Supplementary Information Figure S3

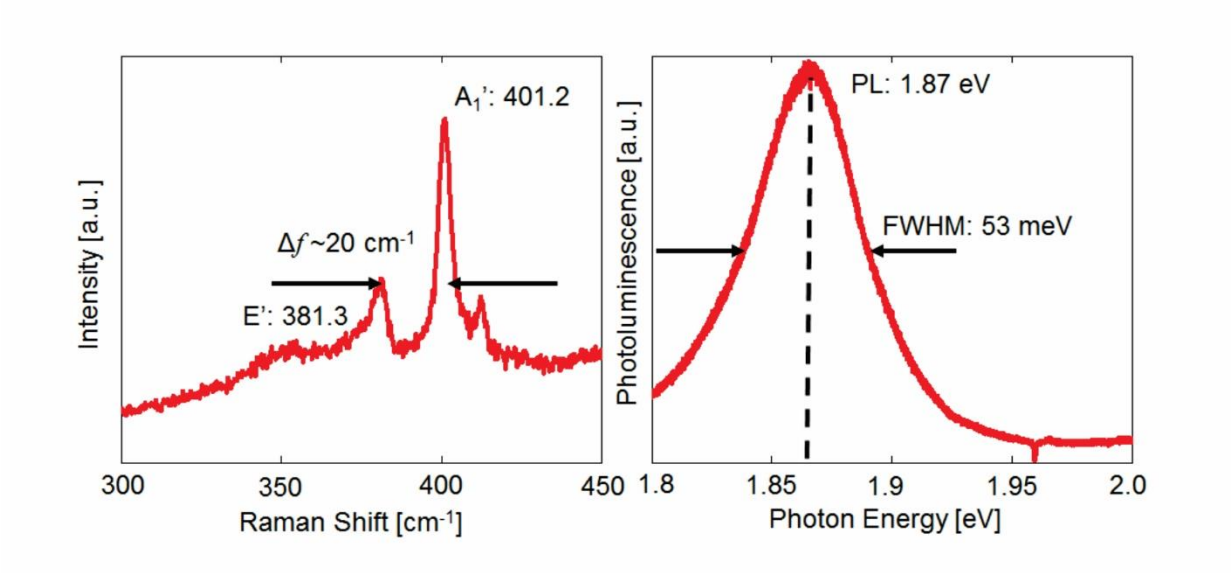

Figure S3. Raman (left) and photoluminescence (right) data for as-grown 1L MoS_2 on sapphire. In the Raman spectrum, the E' and A_1' vibrational modes are near 381 and 401 cm^{-1}, respectively. The PL spectrum has a peak near 1.87 eV and FWHM of 53 meV.

Supplementary Information Figure S4

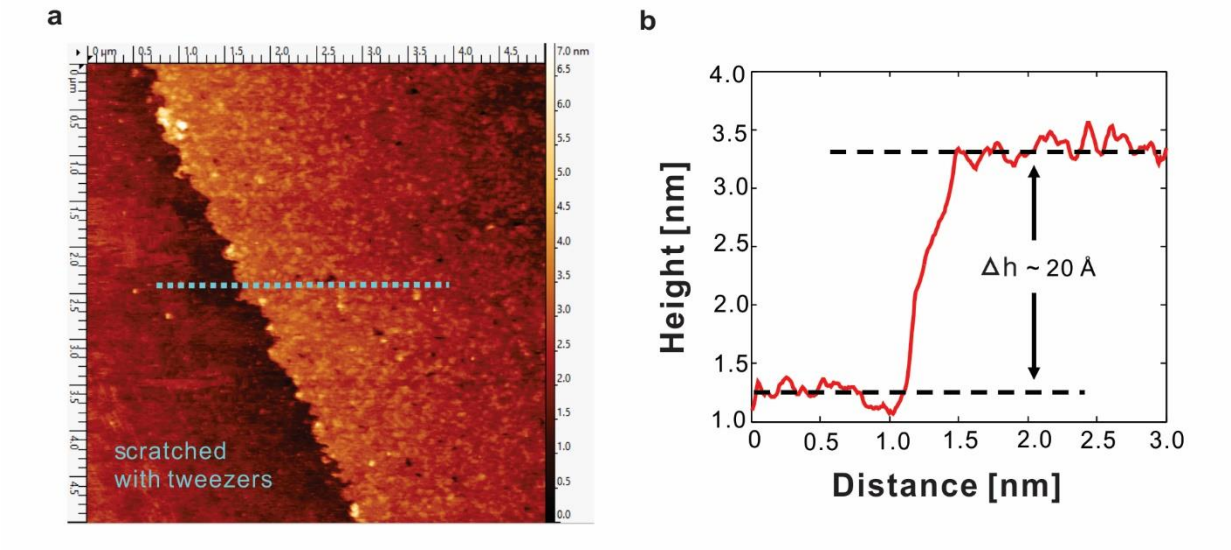

Figure S4. (a) and (b): AFM image and height profile of a continuous growth on SiO_2. The measured step height here is ~20 Å due to the bare surface being made by scratching the MoS_2 away with tweezers.

Supplementary Information Figure S5

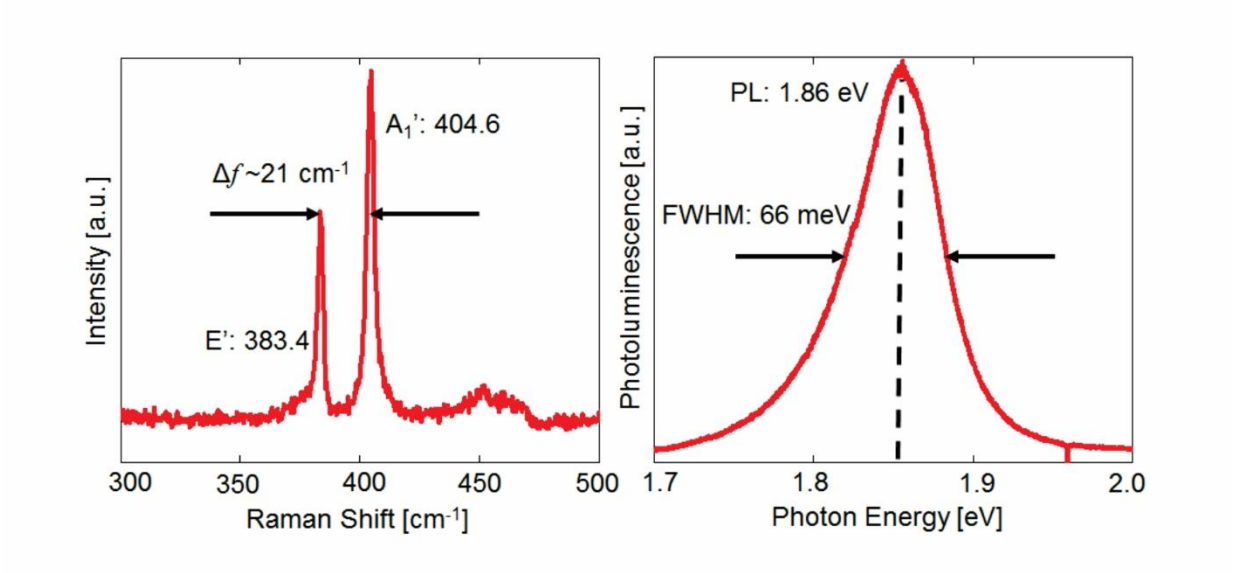

Figure S5. Raman (left) and photoluminescence (right) data for continuous MoS_2 grown on SiO_2. In the Raman spectrum, the E' and A_1' vibrational modes are near 383.5 and 404.5 cm^{-1}, respectively. The PL spectrum has a peak near 1.86 eV and FWHM of 66 meV.

Supplementary Information Figure S6

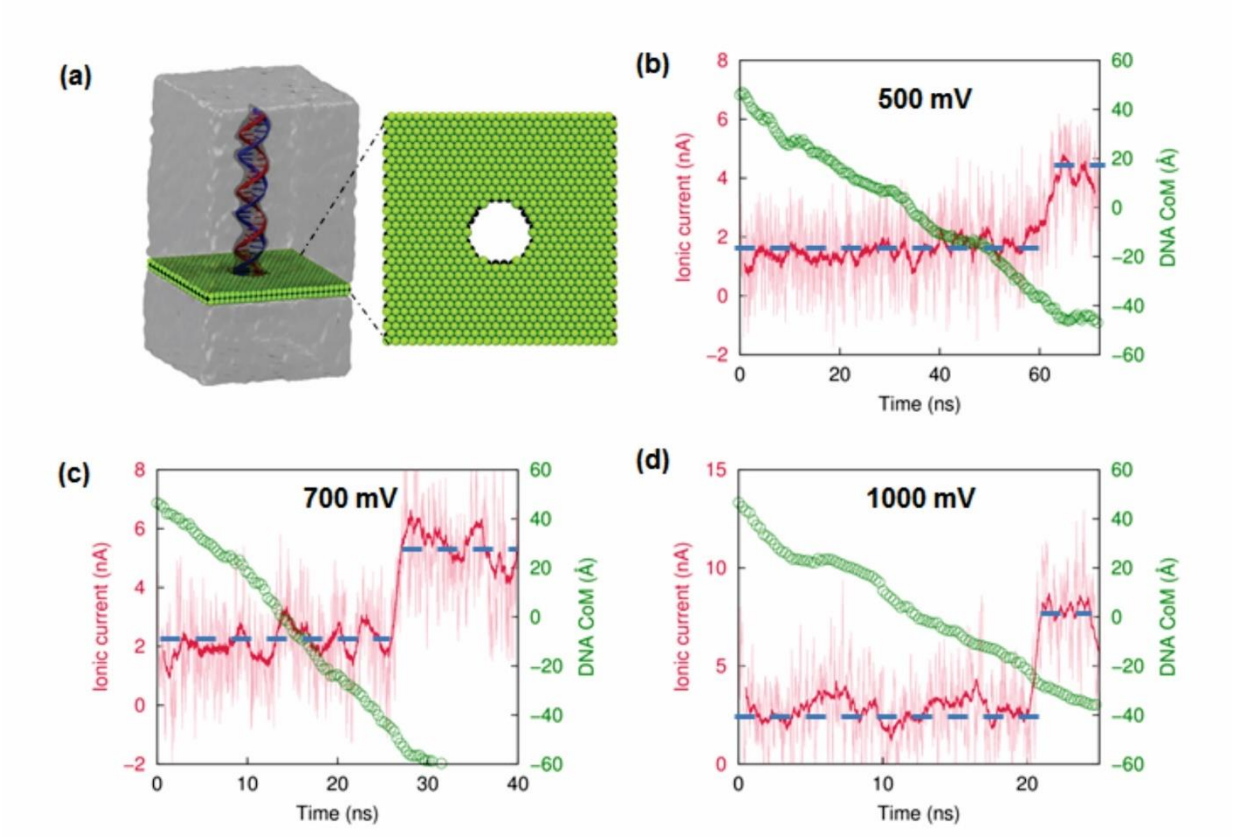

Figure S6. Molecular dynamics simulation of dsDNA translocation through a 2.4 nm diameter MoS_2 nanopore under different voltage biases. (a) Simulation system consisting of a monolayer MoS_2 and a 30 bp long dsDNA strand embedded in a 1 M NaCl solution. (b-c) Recorded ionic current (red) and the center of mass positions of the DNA molecule (green circles) in the direction perpendicular to the MoS_2 membrane when an transmembane voltage 500 (b), 700 (c), 1000 (d) mV was applied to drive the dsDNA translocation through the pore.

To explore the atomic-scale translocation dynamics of a dsDNA through MoS_2 nanopore, we performed three independent molecular dynamics simulations on the system shown in Figure S6a under voltage biases of 500, 700, 1000 mV, respectively. It is found that the recorded ionic current when the pore is occupied by DNA is evidently lower than the open pore current in all the simulations, showing successful detection of DNA translocation (Figure S6c-d), in agreement with our experimental observation.

Supplementary Information Figure S7

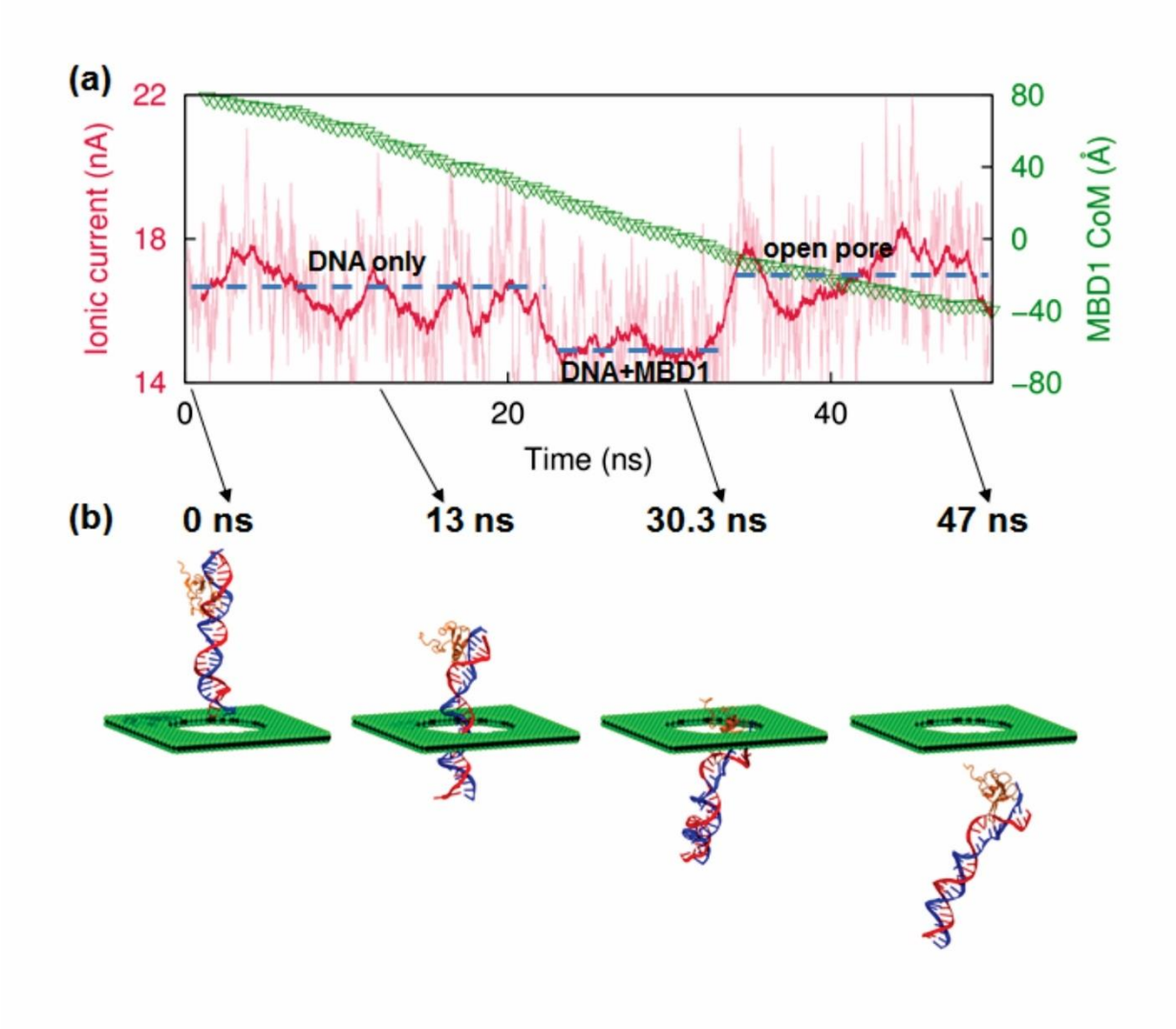

Figure S7. Molecular dynamics simulation of a DNA-MBD1 complex translocation through a 6 nm diameter MoS_2 nanopore under a 500 mV voltage bias. (a) Recorded ionic current (red) and the center of mass position of the MBD1 protein (green triangles) during the translocation of the complex. (b) Snapshots of the MD trajectory at different time instants

We also performed molecular dynamics simulations to study on the atomic-scale the translocation process of a terminal-methDNA/MBD1 complex through a MoS_2 nanopore, as shown in Figure S7. The recoded ionic current exhibits clearly three subsequent levels, ~16.7, ~15 and ~17 nA, induced by the occupation of the pore by DNA only, DNA plus MBD1 protein and nothing (i.e., open pore), respectively. This finding suggests detection of the MBD1 protein and the associated methylation sites.

Supplementary Information Figure S8

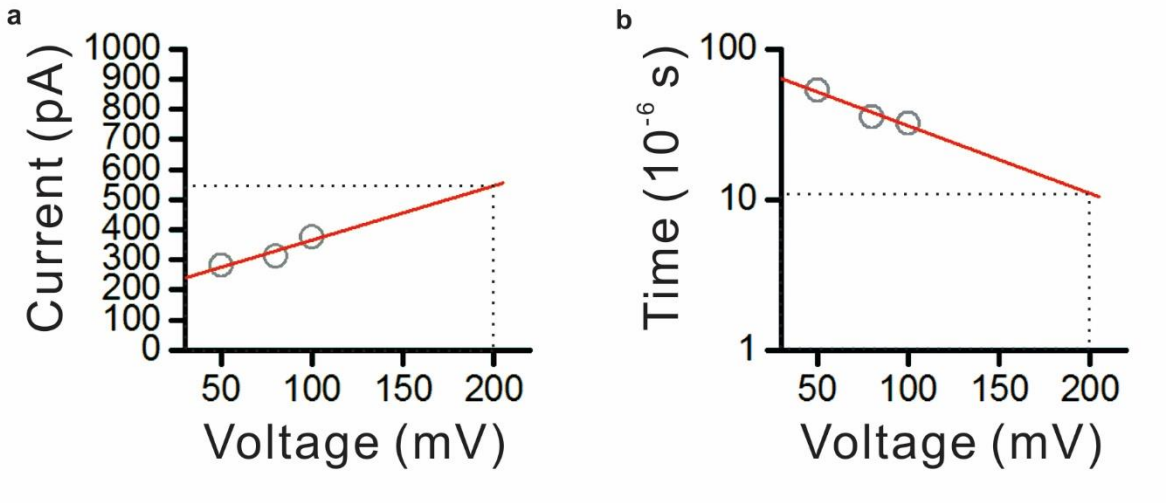

Figure S8. Expected blocked current level and current blockage duration for translocation of 90 bp double-stranded DNA through 7.2 nm MoS_2 nanopore at 200 mV. a. Blocked current at 200 mV was obtained by fitting first-order Polynomial to blocked current values at 50 mV, 80 mV, and 100 mV, and extended the fitting trend to 200 mV. b. Transport duration of 90 bp dsDNA at 200 mV was obtained by fitting Exponential decay function to transport duratin value at 50 mV, 80 mV, and 100 mV, and extended the fitting trend to 200 mV.

Supplementary Information Figure S9

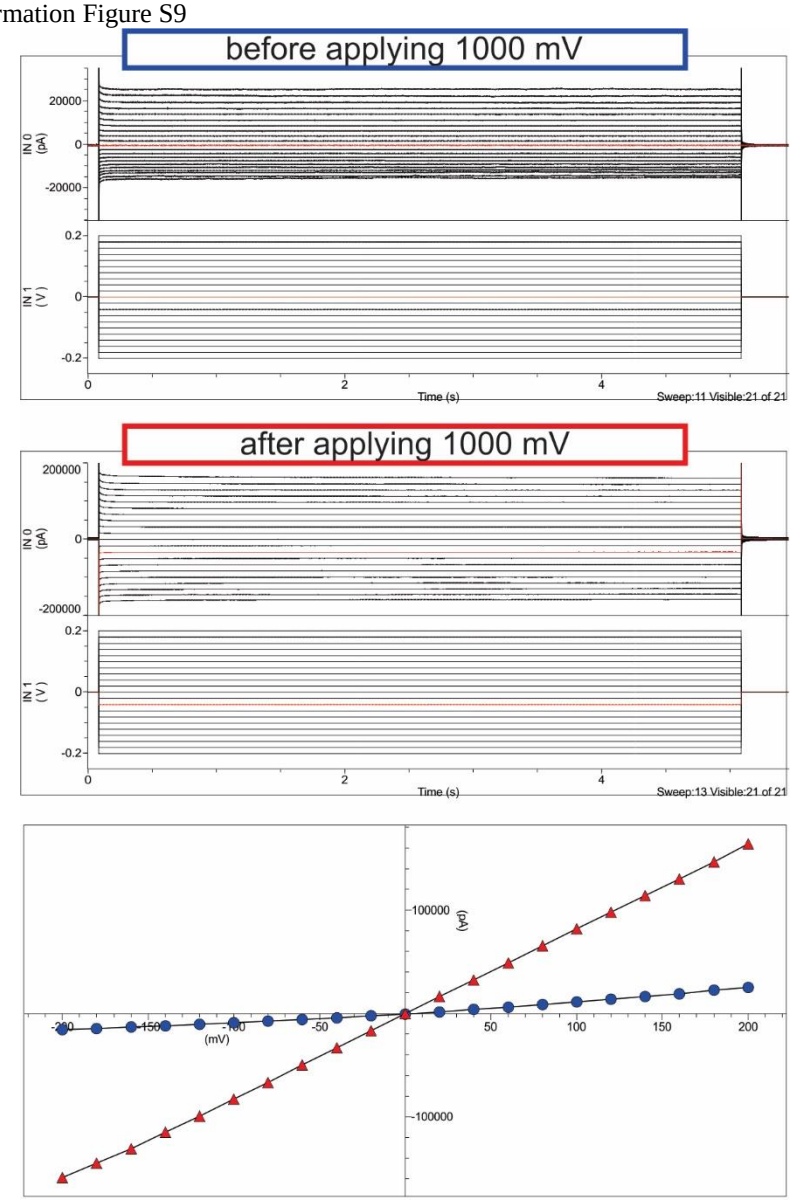

Figure S9. Enlargement of a MoS2 nanopore. The top figure shows the initial IV curve characteristic of a MoS2 nanopore before appying 1000 mV. The middle figure shows the IV curve characteristic of the MoS2 nanopore after exposed at 1000 mV for multiple times. The bottom figure shows the difference of IV characteristic between before and after applying the biased voltage of 1000 mV.

Supplementary References

[S1] K. K. H. Smithe, C. D. English, S. V Suryavanshi, and E. Pop, 2D Mater. **4**, 1 (2017). DOI: 10.1088/2053-1583/4/1/011009.

[S2] D. Dumcenco, D. Ovchinnikov, K. Marinov, P. Lazić, M. Gibertini, N. Marzari, O. L. Sanchez, Y.-C. Kung, D. Krasnozhon, M.-W. Chen, S. Bertolazzi, P. Gillet, A. Fontcuberta i Morral, A. Radenovic, and A. Kis, ACS Nano **9**, 4611 (2015). DOI: 10.1021/acsnano.5b01281.